Available online at www.sciencedirect.com

ScienceDirect

Current Opinion in Electrochemistry

Review Article

Structure–reactivity relationships in Chevrel phase electrocatalysts for small-molecule reduction reactions

Jessica C. Ortiz-Rodríguez and Jesús M. Velázquez

Abstract

Chevrel phases, $M_xMo_6X_8$ (M = metal intercalant, X = chalcogen), constitute a family of materials with composition-dependent physicochemical properties that have shown promising electrocatalytic activity for various small-molecule reduction reactions. The wide range of possible compositions among the Chevrel phase family offers the opportunity to tune the local and electronic structure of discrete Mo_6X_8 cluster units within the extended $M_xMo_6X_8$ framework. Thus, making them an ideal platform for studying structure–function relationships and generating design principles for improved electrocatalytic reactivity. This review summarizes the state of the art in experimental and computational evaluations of Chevrel phases as electrocatalysts for hydrogen evolution, CO_2 reduction, and nitrogen reduction reactions. We aim to elucidate the uncharted small-molecule electrochemical reactivity of Chevrel phases as a function of composition and consequently guide the design of promising multinary chalcogenides for energy conversion reactions.

Addresses

Department of Chemistry, University of California Davis, One Shields Avenue, Davis, CA, 95616, USA

Corresponding author: Velázquez, Jesús M. (jevelazquez@ucdavis.edu)

Current Opinion in Electrochemistry 2022, **34:**101002

This review comes from a themed issue on **Electrocatalysis (2022)**

Edited by **Nicolas Alonso-Vante**

For complete overview about the section, refer Electrocatalysis (2022)

Available online 4 April 2022

https://doi.org/10.1016/j.coelec.2022.101002

Keywords

Chevrel phases (CPs), Multinary chalcogenides, Electrocatalysis, Hydrogen evolution reaction (HER), CO_2 reduction reaction (CO_2RR), Nitrogen reduction reaction (NRR).

Introduction

Materials with tunable compositions offer a platform to study structure–function relations that could lead to design principles for improved catalysis [1–7]. Among the highly-tunable families of materials, Chevrel phases (CPs) have been computationally and experimentally evaluated for various small-molecule electrochemical reduction reactions such as oxygen reduction reaction (ORR) [8–18], hydrogen evolution reaction (HER) [17–25], CO_2 reduction reaction (CO_2RR) [26–32], and nitrogen reduction reaction (NRR) [33]. Figure 1 shows the crystal structure of CPs, which is composed of discrete molybdenum octahedron inside a chalcogen cage with the general formula Mo_6X_8 (X = S, Se, Te). The chalcogen cage and the molybdenum octahedron can be partially substituted (Figure 1a), while the framework forms large cavities that allow the intercalation of metals (Figure 1b).

The highly tunable structure of CPs allows changes in the electronic structure that can influence charge transfer and binding of intermediates at the catalyst surface. Furthermore, geometric structural changes provide diverse chemical environments at the atomic scale with composition-dependent physicochemical properties that can effectively alter reaction pathways [34–37]. Therefore, changes in reactivity and selectivity could be induced through compositional changes. Due to the numerous thermodynamically accessible CP compositions, improved catalysts' design will benefit from identifying properties that can describe and predict catalytic performance, coined reactivity descriptors. Hence, reactivity descriptors such as the d-band model used to describe bond formation on transition-metal surfaces [38–40], and the bulk-phase oxygen p-band center used to describe ORR on perovskite cathodes [6,41,42] have shown to enable the design of new catalysts and facilitate the screening of high-throughput catalysts [43].

While the changes in reactivity and selectivity as a function of composition have been widely reported for ORR in CPs [44–49], analogous literature for other electrochemical small-molecule reduction reactions remain scarce. This review provides an overview of the computational and experimental efforts to elucidate the electrocatalytic activity of CPs for HER, CO_2RR, and NRR. Given the inherent complexity of the aforementioned reactions, the scope of this review is narrowed to the current knowledge on the interactions at the bulk surface–adsorbate interface (e.g., H adsorption and CO hydrogenation) that dominate electrochemically driven reaction pathways. Through our discussion, we aim to

Figure 1

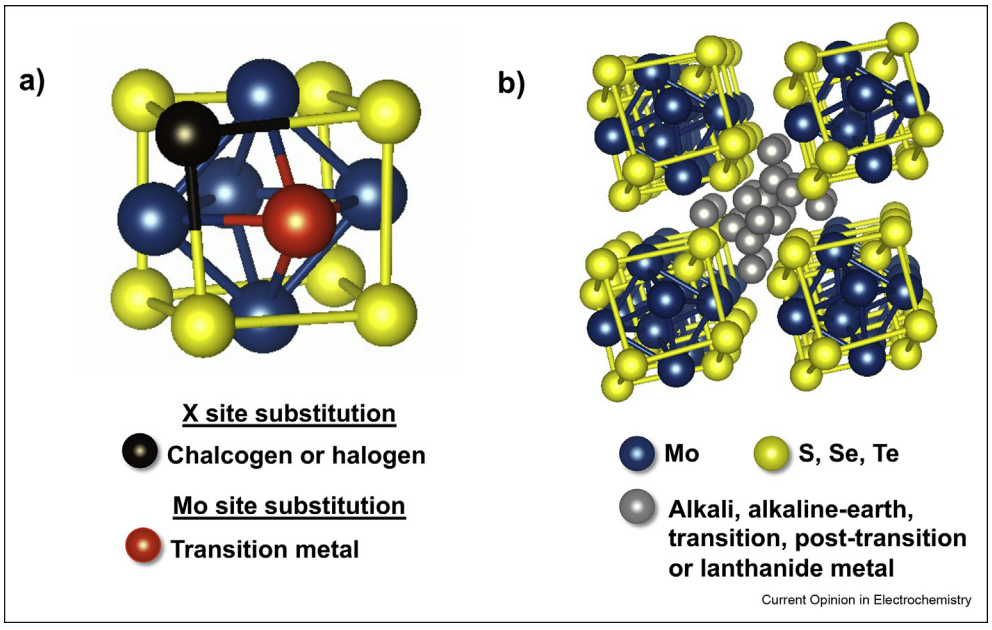

(**a**) CP structure depicting the possible partial substitutions in the Mo_6X_8 cluster and (**b**) the cavities formed between clusters which allow the intercalation of a variety of metals.

elucidate factors in the electronic structure that preferentially favor interactions with reaction intermediates for HER, CO_2RR, or NRR (structure–function relationships), as well as reactivity trends as a function of composition for each of the reactions of interest (structure–reactivity relationships). We intend that the compendium of literature included stimulates the further study of CPs, expanding their composition design and electrocatalytic evaluation.

CPs as HER catalyst

Since their discovery, CPs have been extensively evaluated as HER catalysts [17–25]. As shown in Table 1, HER relies on the ability of the catalytic surface to adsorb H, making the adsorption/desorption behaviors of the solid surface a crucial property in HER catalysis [50,51].

Theoretical studies under various reaction conditions agree that H adsorption (H_{ads}) interactions in CPs occur through the chalcogen–molybdenum bridging site [22,31,32,52]. A recent investigation by Ortiz-Rodríguez et al. [22] has supported such results by elucidating changes in the HER activity of CPs as a function of chalcogen (Mo_6X_8, X = S, Se, Te) in acidic media. Figure 2a shows the polarization curves for polycrystalline CP powders deposited on a carbon substrate. The decrease in overpotential to achieve a current density of 10 mA cm^{-2}_{ECSA} indicates an increase in the HER activity as the Lewis basicity of the X_8 chalcogen cage increases. The reactivity trend was explained by the decrease in X–H distance as well as the improved H_{ads} energy calculated for the CP sulfide compared to the selenide and telluride phases. Such changes are illustrated in Figure 2b where H_{ads} occurs farther from the chalcogen as the electronegativity of the chalcogen decreases (H–S<H–Se<H–Te). Furthermore, Mo_6S_8 maintained a steady time-dependent overpotential at a current density of 10 mA cm^{-2} over 48 h.

It was concluded that the changes in H stabilization are influenced by changes in the local bonding environment (local effect) and the bulk electronic structure as a function of chalcogen (electronic effect), which can be described using the simplified orbital representation in Figure 3. Hughbanks and Hoffmann [53] elucidated that the frontier orbitals of CPs are formed by twelve bonding and eighteen antibonding orbitals, primarily Mo d in character. The relative positions and the width of the d bands are strongly influenced by the covalent

Table 1

HER mechanism in acidic electrolyte.

Acidic electrolyte	
$2H^+_{(aq)} + 2e^- \rightarrow H_{2(g)}$	
Volmer step	$H^+ + e^- \rightarrow H_{ads}$
Tafel step	$2H_{ads} \rightarrow H_2$
Heyrovsky step	$H^+ + H_{ads} + e^- \rightarrow H_2$

Figure 2

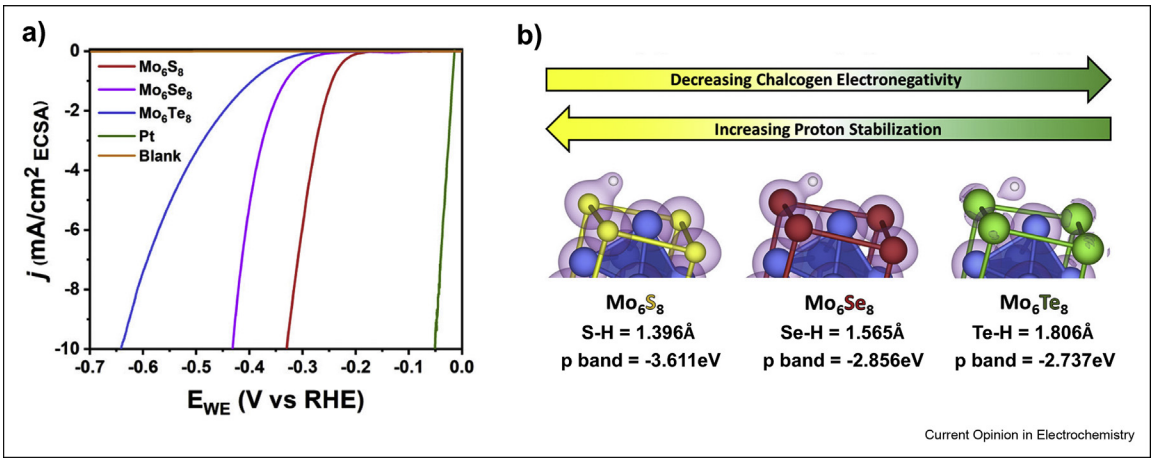

(**a**) HER polarization curves for CP chalcogenide electrodes in 0.5 M H_2SO_4, along with 20% Pt/C on Vulcan Carbon Cloth and a blank (carbon paper with PTFE/carbon black/IPA ink) for comparison. (**b**) Graphical representation of the changes in H_{ads} interactions as a function of chalcogen along the calculated X–H bond distances and corresponding p band center. Copyright 2020 American Chemical Society. Figure reproduced with permission from Ortiz-Rodríguez et al. [22].

Figure 3

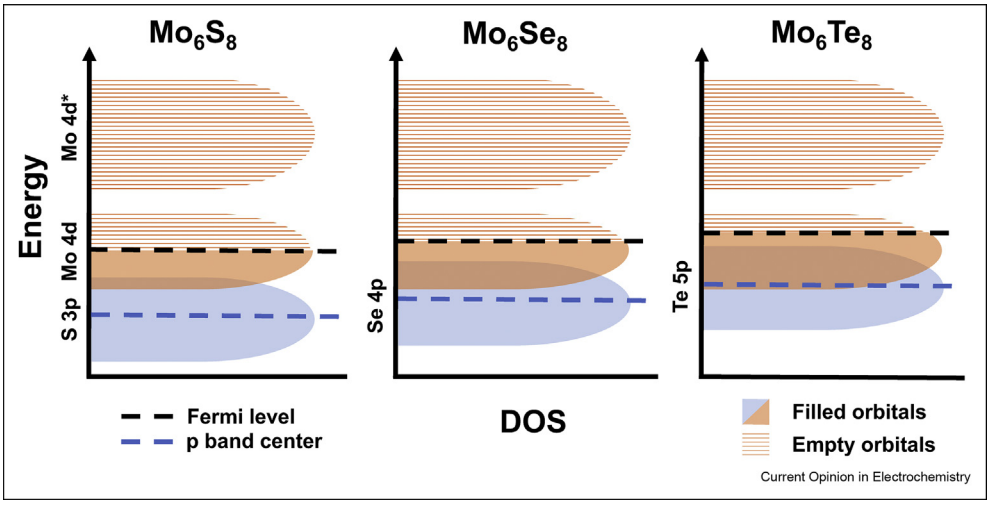

Simplified representation of the frontier orbital interactions of CP chalcogenides based on the studies by Schubert et al., Hughbanks et al., Singstock et al., Lilova et al. [18,54,55,56]. The slight increase in the density of states at the Fermi level as the electronegativity of the chalcogen decreases is caused by a decrease in the formal charge of the chalcogen [55–61].

mixing with the X p states, which decreases in the sequence Mo_6S_8< Mo_6Se_8< Mo_6Te_8 [54]. The lower 3p sulfur orbitals of Mo_6S_8 shown in Figure 3 have a higher p character which improves the H–S orbital overlap and allows the favorable stabilization of H at the chalcogen site (local effect). Likewise, the increase in energy of the chalcogen p orbitals leads to a higher p band center (Figure 3, dashed blue line) which scales inversely with the observed HER overpotentials (electronic effect). Therefore, the observed reactivity trend suggests that in binary CPs the position of the p-band center is a useful descriptor to predict their HER activity, which has also been the case for other recent HER catalyst [62–65].

Metal-intercalated and Mo_6 octahedron substituted CPs have also been evaluated as HER catalyst [17,18,20,24,25]. By evaluating various metal-intercalated and octahedron substituted CPs, Shubert and Tributsch [20] identified that the single most active metal center favors HER. That is, either the Mo of the Mo_6-octahedron or the

intercalated/substituted metal determines the catalytic activity. Figure 4 shows the results that lead to this conclusion. The authors evaluated the exchange current (i_0) and overpotential (η) of various polycrystalline CPs with the same figures of merit for monometallic electrodes of the corresponding intercalated/substituted metal in acidic media (e.g., $CdMo_6S_8$/Cd; $Mo_2Re_4S_8$/Re). To identify the active center for HER, correlations between the i_0 and η of CPs and the monometallic electrodes were made. It was noticed that although the i_0 and η varied continuously for each monometallic electrode (x axis), multiple CPs share the same i_0 and η value (y axis). The shaded areas indicate CPs with statistically identical i_0 and η values while the values for their corresponding metal intercalant (Cd, In, Pb, Sn, Zn, Cu, Mo) change. Thus, it is believed that the Mo octahedron is mainly responsible for proton reduction in this case as if the metal intercalant was the active center, the i_0 and η values for the CPs will vary. In contrast, deviations from the shaded area suggest that the intercalated or substituted metal strongly influences the catalytic activity as the i_0 and η for the CP and the monometallic electrode change continuously.

Based on these results, HER activity is directed by the Mo octahedron for MMo_6S_8 (M = Cd, In, Pb, Sn, Zn, Cu_2), which all have a lower HER activity than Mo_6S_8. The trend observed is further exemplified by the descriptors elucidated by Ortiz-Rodriguez et al. [22] since higher p-band centers are expected upon metal intercalation due to the electron donation from the metal intercalant to the chalcogen [30,66–68]. Interestingly, the intercalated or substituted metal dominates HER activity in MMo_6S_8 (M = Ag, Pd) and $Mo_2Re_4S_8$. The improved HER activity of these CPs compared to Mo_6S_8 suggest the direct participation of the intercalated/substituted metal as an active site for H_{ads}. However, further evaluations that elucidate changes in proton adsorption as the chemical environments that influence HER activity change (intercalated/substituted metal or Mo octahedron) remain to be performed.

Recent efforts to improve the HER activity of CPs have been focused on the design of nanoscale CPs [19,21,23]. A comparison between bulk and nanoparticulate Mo_6S_8 in acidic media shows an increase in the HER activity as the surface area-to-volume increases as well as structural stability after 1000 voltammetry cycles [19]. Nanoscale Mo_6S_8 also shows an improved HER activity to nanoscale MMo_6S_8 (M = Cu, Zn), which agrees with the results obtained by Shubert and Tributsch [20]. Improvements in the catalytic activity of CP nanoparticles have also been observed by the inclusion of carbon additives in the catalyst electrode [23,24]. Although these approaches have shown to successfully enhance the HER activity of CPs, significant improvements could be made by atomically identifying the most active surface sites(s) in CP nanoparticles and generating synthetic approaches that could preferentially yield such active site ensembles. Likewise, fewer reports have evaluated the HER activity of CPs in alkaline media, which have shown promising electrocatalytic activity and stability under these conditions [21,25]. Therefore, the reactivity trends discussed remain to be further evaluated in alkaline reaction conditions.

CPs as CO_2RR and NRR catalyst

Favorable intermediates energies are predicted for the reduction of CO_2 to methanol in Mo_6S_8 and metal-

Figure 4

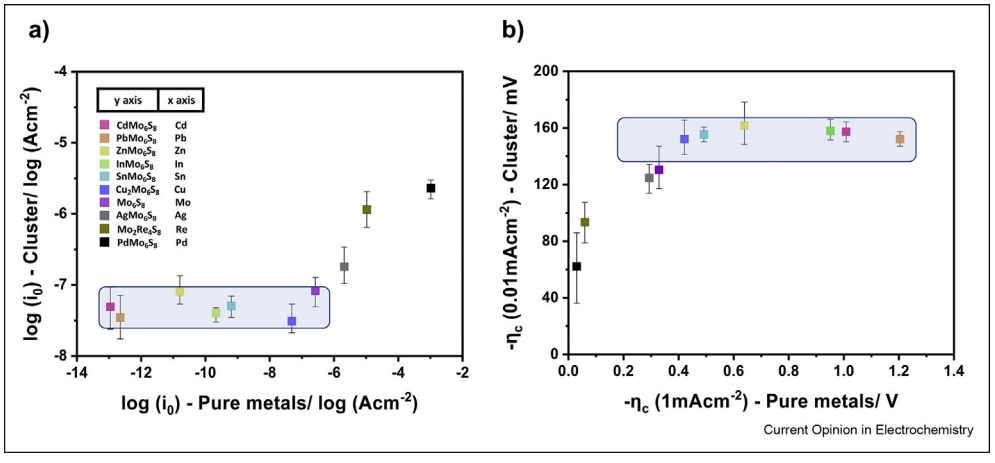

(**a**) Correlation between log (i_0) of CPs and log (i_0) of monometallic electrodes of the corresponding intercalated/substituted metal. (**b**) Correlation between η of CPs and the η of monometallic electrodes of the corresponding intercalated/substituted metal. CP electrodes contained polycrystalline CP powders, graphite powder (improve conductivity) and nujol (pasting medium). Shaded area includes materials in which the Mo-octahedron is strongly dominating the reduction mechanism. Data obtained from Schubert et al. [20].

Figure 5

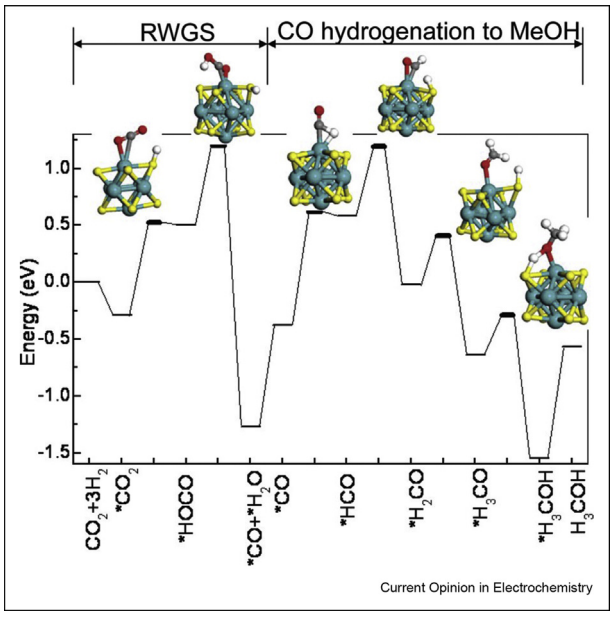

Optimized potential energy diagram for methanol synthesis from CO_2 and H_2 on a Mo_6S_8 cluster. Thin bars represent the reactants, products, and intermediates; the thick bars stand for the transition states (Mo, cyan; S, yellow; C, gray; O, red; H, white). Copyright 2009 American Chemical Society. Figure reproduced with permission from Liu et al. [31].

intercalated CPs [29,31] following the chemical equation:

$$CO_2 + 6H^+ + 6e^- \rightarrow CH_3OH + H_2O$$

As shown in Figure 5, CO_2RR intermediates are predicted to interact at the Mo sites in Mo_6S_8 preferentially, whereas S atoms facilitate H–H bond cleavage by forming relatively strong S–H bonds [31]. The addition of metal intercalants and substitutions in the Mo octahedron are expected to change the interactions of CO_2RR intermediates compared to Mo_6S_8; however, H_{ads} still preferentially occurs through chalcogen interactions [26–29,32]. Figure 6 shows the expected influence of metal intercalants in the CO_2RR mechanism of CPs, which includes interactions through modifications in the electronic structure (ligand effect) or participation of the metal intercalant as an active site (ensemble effect) [29].

Perryman et al. [30] experimentally validated the CO_2RR activity of CPs elucidated by theory. This study evaluated the ability of polycrystalline Mo_6S_8, $Cu_2Mo_6S_8$, $Ni_2Mo_6S_8$, and $Cr_{1.73}Mo_6S_8$ to reduce CO_2 and CO in 0.1 M Na_2CO_3 and 0.1 M $NaHCO_3$, respectively. Electrochemical results followed by gaseous and liquid product analysis show that all CPs reduced CO_2 to only methanol and formate in the liquid phase, while H_2 production had the highest faradaic efficiency. The electrocatalytic performance of $Cu_2Mo_6S_8$ was maintained over the course of multiple hours of electrolysis, even at a reductive potential of -1 V versus RHE. Furthermore, the selectivity of $Cu_2Mo_6S_8$ towards methanol production was increased when CO was introduced as the target for reduction, which circumvents formate production. These results suggest that the pathway for methanol production on $Cu_2Mo_6S_8$ catalysts does proceed via CO hydrogenation following the predicted mechanism for CO_2RR in Mo_6S_8 [31] (Figure 5). Therefore, the dominance of the ligand effect over the ensemble effect is expected for $Cu_2Mo_6S_8$, but further operando experiments are needed to confirm this hypothesis.

Figure 6

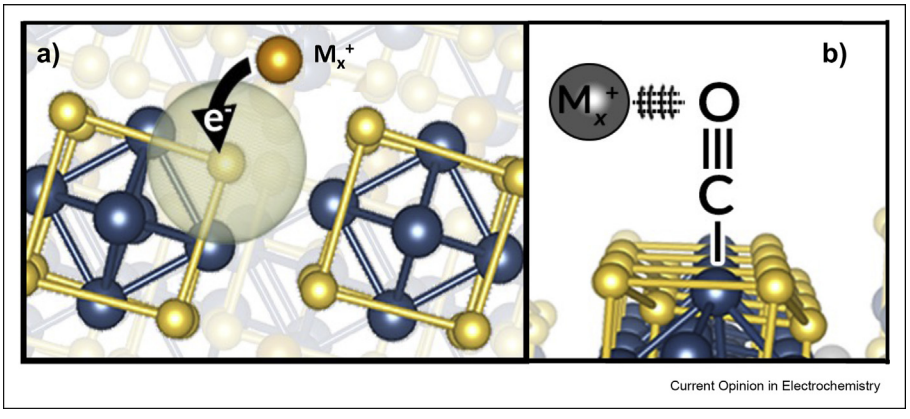

Electrocatalytic (**a**) ligand and (**b**) ensemble effect of metal intercalants in the CP structure.

Figure 7 shows the changes in the electronic structure upon Cu intercalation into the Mo_6S_8 cluster obtained through X-ray Absorption Near-Edge Structure (XANES). The minimal shift in the Mo K-edge absorption observed for Mo_6S_8 and $Cu_2Mo_6S_8$ in Figure 7a indicates an insignificant change in the electronic structure of the Mo, which is predicted to be crucial in the stabilization of CO_2RR intermediates [26–29,31,32]. The intercalation of Cu seems to preferably influence the electronic structure of the chalcogen cage as it fills available S 3p orbitals causing a decrease in the S K pre-edge shoulder (~2471 eV) of $Cu_2Mo_6S_8$ compared to Mo_6S_8 (Figure 7b). Following the previous discussion regarding H_{ads} interactions, the electronic changes induced by Cu intercalation could influence H_{ads} at the S–Mo bringing site rather than CO_2RR intermediates at the Mo site, which could be a topic of interest for future studies.

An alternative to increase methanol production in CPs could be to increase the d-band electron density, which has been shown to increase the activity of CPs for ORR. Vante et al. [17] evaluated different Mo-containing compounds in which the concentration of d electrons changes by rising the Fermi level when going from the Mo cluster (Mo_6Se_8) to the substituted ones ($Mo_4Ru_2Se_8$/$Mo_2Re_4Se_8$). As shown in Figure 8, partial substitution of the Mo octahedron by Re or Ru raises the valency electron concentration in the cluster from $20e^-$ to $24\ e^-$, which increases the occupation of metal d states near the Fermi level while the chalcogen electronic structure is minimally altered [69–71] (Figure 8). Such electronic changes have been shown to significantly improve the ORR activity of CPs [9,11,15,44]. The poor ORR catalytic properties of

Figure 8

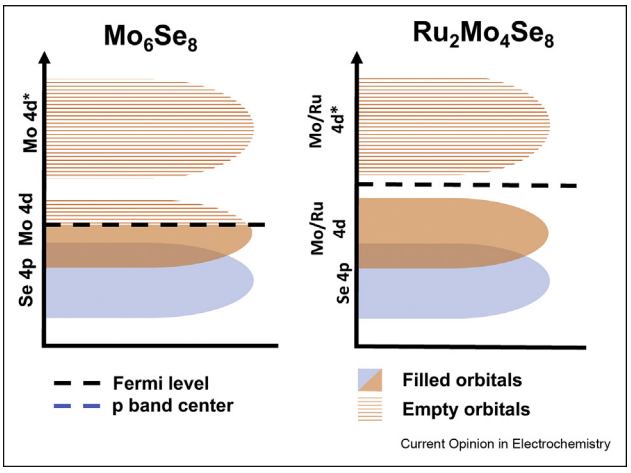

Simplified representation of the changes in frontier orbital interactions for Mo_6Se_8 and $Ru_2Mo_4Se_8$ based on the studes by Alonso Vante et al., Jaegermann et al., Jaegermann et al.[9,44,71].

Mo_6Se_8 compared to $Mo_4Ru_2Se_8$/$Mo_2Re_4Se_8$ can be related to the small metal d-density at the Fermi edge, which decreases the stabilization of oxygen intermediates [15,44,48]. Similar to what is predicted for CO_2, molecular oxygen interacts preferentially with the metallic centers at the octahedron, therefore the evaluation of CPs with increased metal d-density at the Fermi edge could lead to improved CO_2RR catalytic activity.

Lastly, computational calculations can also assist in designing CPs with improved CO_2RR efficiencies.

Figure 7

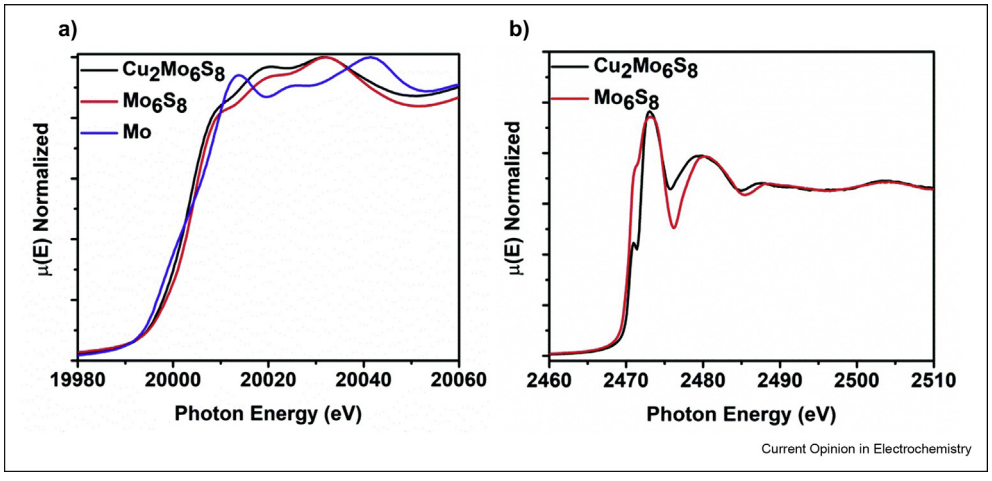

(**a**) K-edge XANES for Mo in $Cu_2Mo_6S_8$ and Mo_6S_8, with Mo^0 foil for reference. (**b**) K-edge XANES for S in $Cu_2Mo_6S_8$ and Mo_6S_8. Copyright 2020 Royal Society of Chemistry. Figure reproduced with permission from Perryman et al. [30].

Figure 9

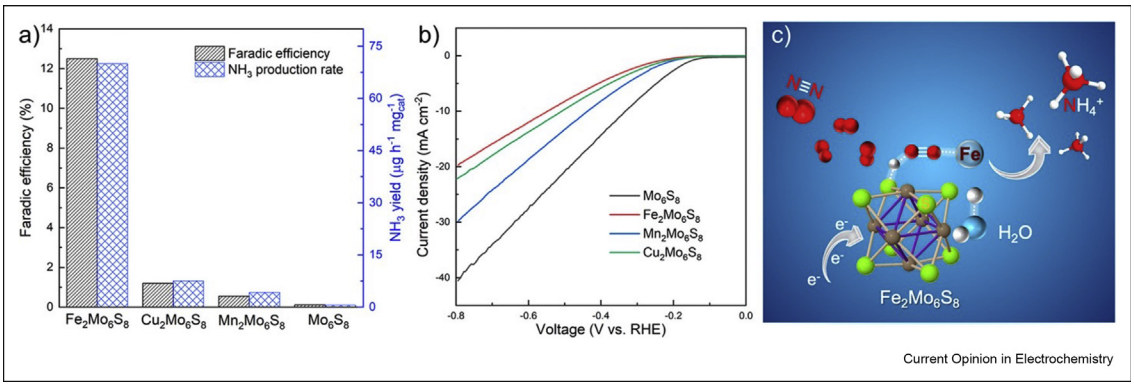

(**a**) Comparison of N_2 to NH_3 conversion efficiency and average NH_3 production rate for Mo_6S_8 and $M_2Mo_6S_8$ (M = Fe, Mn, and Cu) electrocatalysts in aqueous electrolyte (0.5 M Na_2SO_4/0.1 M sodium citrate buffer). (**b**) Linear sweep voltammetry (LSV) curves for hydrogen evolution in Ar-saturated electrolyte. (**c**) Schematic illustration of the proposed binding mechanism for N_2 absorption and subsequent conversion to NH_3. Copyright 2021 American Chemical Society. Figure reproduced with permission from Lu et al. [33].

KMo_6S_8 has been predicted to facilitate CO_2 to methanol conversion due to a strong ensemble effect of K, which could stabilize CO_2 intermediates through electrostatic interactions and lower the corresponding transition states involving H_xCO_y radicals [29]. Single-atom catalysis on CPs [26,27,52] and other metal intercalated CPs [28,32,72] have also been computationally evaluated as CO_2 and CO conversion catalysts, showing promising C_1 and C_2 products. However, there is currently no experimental evidence to confirm such predictions. It is important to mention that most of the computational studies discussed do not consider structural effects such as the synthetic accessibility of CPs [73,74], changes in cavity occupancy as a function of metal intercalant stoichiometry and/or identity [73,75–77], metal intercalant mobility [78–80], and metal de-intercalation upon applied potential [18]. Therefore, there is a broad opportunity to experimentally validate computational predictions and study other structural effects not considered by theory.

Although NRR has been less studied in CPs, experimental results strongly suggest that the ensemble effect dominates the reaction. Lu et al. [33] evaluated polycrystalline Mo_6S_8, $Cu_2Mo_6S_8$, $Mn_2Mo_6S_8$, and $Fe_2Mo_6S_8$ as electrocatalysts for the conversion of N_2 to NH_3 in aqueous solution (pH ~4.6), following the chemical equation:

$$N_2 + 6H^+ + 6e^- \rightarrow 2NH_3$$

An increase in faradaic efficiency and NH_3 production rate was observed in metal-intercalated CPs, being $Fe_2Mo_6S_8$ the best performing catalyst (Figure 9a). The intercalation of Fe into the CP cluster also increased the overpotential for the competing HER (Figure 9b) leading to the increased NRR selectivity. In addition, chronoamperometric responses for $Fe_2Mo_6S_8$ at potentials ranging from −0.15 V to −0.40 V versus RHE show stable currents for the 2hr testing period. It was concluded that Fe must participate in the absorption and/or conversion of N_2, while Mo and S atoms alone are unable to activate N_2. The proposed mechanism for N_2 conversion on $Fe_2Mo_6S_8$ is shown in Figure 9c in which Fe directly interacts with N_2 while the chalcogen sites are expected to assist in H_{ads}. Further improvements in catalytic activity will highly benefit from computational work that unravels the NRR mechanism on $Fe_2Mo_6S_8$ and could identify ways to enhance intermediate stabilization.

Conclusion and outlook

This review emphasized the adsorption of key intermediates in CPs under HER, CO_2RR, and NRR conditions as well as their composition-dependent electrochemical properties. The discussion highlights the compositional control over orbital population, orbital symmetry, and intermediate adsorption strength in CPs which provide a platform to generate transferable principles for improved catalyst design. Among those, we highlight the influence of the local and electronic structure in the HER activity of CPs as well as the predicted ligand and ensemble effects that dominate reaction trajectories in CO_2RR, and NRR. Several routes to improve the electrocatalytic activity of CPs are proposed, considering computational and experimental efforts that elucidate electrochemical small-molecule reactivity.

As the electrochemical evaluation of CPs for energy conversion reactions moves forward, it is imperative to unravel the structural changes at the catalyst interface

under an electrochemical environment in order to generate reactivity descriptors that extend from the bulk electronic properties discussed. To this end, we suggest the incorporation of in situ/operando experimentation such as in situ atomic scale scanning transmission electron microscopy (STEM) [81,82], electrochemical scanning tunneling microscopy (ECSTM) [83,84] and in situ/operando synchrotron-based X-ray techniques to understand changes at the electrode−electrolyte interface [85,86]. Likewise, the incorporation of electroanalytical techniques such as scanning electrochemical microscopy (SECM) [87,88], differential electrochemical mass spectrometry (DEMS) [89−91] and in-situ electrochemical Fourier transform infrared spectroscopy (FTIR) [92−94] will enable direct probing of the local activity and improve the current mechanistic understanding of CO_2RR and NRR on the CP interface by allowing the detection of key intermediate species beyond those included herein.

Besides the inherent challenges of applying the suggested techniques to fully understand the electrocatalytic activity of CPs [95−97], it is essential to develop alternative synthetic approaches that would generate well-defined CP nanoparticles and thin films which allow the proper characterization of the outermost atomic layer of CPs at which intermediate adsorption and charge transfer interactions take place. The latter is specifically important when considering spectroscopy techniques in which the penetration depth of the emission source will lead to contributions from the bulk and surface electronic structure [86,98,99]. Lastly, a systematic evaluation of catalytic activity as a function of reaction conditions (e.g., pH, electrolyte ions, crystallinity of the electrode), as well as long-term stability measurements, must be evaluated for future comparisons with state-of-the-art electrocatalysts. We expect that the comprehensive conceptualization in this review reveals the underexplored potential of CPs as a highly tunable platform to study composition-dependent reactivity trends and generate design principles for improved catalyst design.

Author contributions

JOR and JMV contributed to the conception and design of the study. JOR drafted the article. All authors have reviewed, edited, and given approval to the final version of the manuscript.

Funding sources

We would like to thank the University of California, Davis for start-up funding, as well as support from the Cottrell Scholar program supported by the Research Corporation for Science Advancement (RCSA 26780). JMV also acknowledges funding support from the NSF through the Faculty Early Career Development Program (DMR-2044403). JOR was funded by the National Science Foundation Graduate Research Fellowship (NSF 1650042).

Notes

The authors declare no competing financial interest.

Declaration of competing interest

The authors declare that they have no known competing financial interests or personal relationships that could have appeared to influence the work reported in this article.

Acknowledgments

We gratefully acknowledge Brian Wuille Bille for assisting in the design of the table of contents image.

References

Papers of particular interest, published within the period of review, have been highlighted as:

* of special interest
** of outstanding interest

1. Perryman JT, Velázquez JM: **Design principles for multinary metal chalcogenides: toward programmable reactivity in energy conversion**. *Chem Mater* 2021, **33**:7133−7147, https://doi.org/10.1021/acs.chemmater.1c01983.

2. Wang X, Wang C, Ci S, Ma Y, Liu T, Gao L, Qian P, Ji C, Su Y: **Accelerating 2D MXene catalyst discovery for the hydrogen evolution reaction by computer-driven workflow and an ensemble learning strategy**. *J Mater Chem A* 2020, **8**: 23488−23497, https://doi.org/10.1039/d0ta06583h.

3. Tatarchuk T, Al-Najar B, Bououdina M, Aal Ahmed MA: **Catalytic and photocatalytic properties of oxide spinels**. In *Handbook of ecomaterials*. Springer International Publishing; 2019: 1701−1750, https://doi.org/10.1007/978-3-319-68255-6_158.

4. Zhang Z, Zhu Q, Sadakane M, Murayama T, Hiyoshi N, Yamamoto A, Hata S, Yoshida H, Ishikawa S, Hara M, Ueda W: **A zeolitic vanadotungstate family with structural diversity and ultrahigh porosity for catalysis**. *NatCommun* 2018, **9**:3789, https://doi.org/10.1038/s41467-018-06274-2.

5. Löffler T, Meyer H, Savan A, Wilde P, Garzón Manjón A, Chen YT, Ventosa E, Scheu C, Ludwig A, Schuhmann W: **Discovery of a multinary noble metal−free oxygen reduction catalyst**. *Adv Energy Mater* 2018, **8**:1802269, https://doi.org/10.1002/aenm.201802269.

6. Suntivich J, May KJ, Gasteriger HA, Goodenough JB, Shao-Horn Y: **A perovskite oxide optimized for oxygen evolution catalysis from molecular orbital principles**. *Science* 2011, **334**: 1380−1383, https://doi.org/10.1126/science.1211927.

7. Reed DA, Hochuli TJ, Gadjieva NA, He S, Wiscons RA, Bartholomew AK, Champsaur AM, Steigerwald ML, Roy X, Nuckolls C: **Controlling ligand coordination spheres and cluster fusion in superatoms**. *J Am Chem Soc* 2021, **144**: 306−313, https://doi.org/10.1021/jacs.1c09901.

8. Xia F, Li B, Liu Y, Liu Y, Gao S, Lu K, Kaelin J, Wang R, Marks TJ, Cheng Y: **Carbon free and noble metal free Ni2Mo6S8 electrocatalyst for selective electrosynthesis of H2O2**. *Adv Funct Mater* 2021, **31**:2104716, https://doi.org/10.1002/adfm.202104716.

9. Alonso Vante N, Jaegermann W, Tributsch H, Hónle W, Yvon K: **Electrocatalysis of oxygen reduction by chalcogenides containing mixed transition metal clusters**. *J Am Chem Soc* 1987:3251−3257, https://doi.org/10.1021/ja00245a013.

10. Fisher C, Alonso Vante N, Fiechter STH: **Electrocatalytic properties of mixed transition metal tellurides (Chevrel-phases) for oxygen reduction**. *J Appl Electrochem* 1995, **25**: 1004−1008, https://doi.org/10.1007/BF00241948.

11. Malakhov Iv, Nikitenko SG, Savinova ER, Kochubey DI, Alonso Vante N: **In situ EXAFS study to probe active centers of Ru chalcogenide electrocatalysts during oxygen reduction reaction**. *J Phys Chem B* 2002, **106**:1670–1676, https://doi.org/10.1021/jp011295l.

12. Alonso Vante N, Tributsch H, Solorza-Feria O: **Kinetics studies of oxygen reduction in acid medium on novel semiconducting transition metal chalcogenides**. *Electrochim Acta* 1995, **40**:567–576, https://doi.org/10.1016/0013-4686(94)00377-D.

13. Ellmw K, Giersig M, Alonso Vante N: **Novel low-temperature synthesis of semiconducting transition metal chalcogenide electrocatalyst for multielectron charge transfer: molecular oxygen reduction**. *Electrochim Acta* 1994, **39**:1647–1653, https://doi.org/10.1016/0013-4686(94)85149-2.

14. Schubert B, Alonso Vante N, Gocke E, Tributsch H: **Oxygen reduction electrocatalysis by Chevrel Phase sulfides supported on carbon paste electrodes**. *Phys Chem* 1988, **92**:1279–1283, https://doi.org/10.1002/chin.198904021.

15. Alonso Vante N, Fieber-Erdmann M, Rossner H, Holub-Krappe E, Giorgetti C, Tadjeddine A, Dartyge E, Fontaine A, Frahm R: **The catalytic centre of transition metal chalcogenides vis-à-vis the oxygen reduction reaction : an in situ electrochemical EXAFS study**. *J Phys IV* 1997, **7**:887–889, https://doi.org/10.1051/jp4:1997266ï.

16. Alonso Vante N, Tributsch H: **Energy conversion catalysis using semiconducting transition metal cluster compounds**. *Nature* 1986, **323**:431–432, https://doi.org/10.1038/323431a0.

17. * Alonso Vante N, Schubert B, Tributsch H, Perrinf A: **Influence of d-state density and chemistry of transition metal cluster selenides on electrocatalysis**. *J Catal* 1988, **112**:384–391, https://doi.org/10.1016/0021-9517(88)90152-2.
The authors explored how the d-state density influenced the ORR and HER activity of various CPs. This is one of the first identifications of reactivity descriptors to improve the electrocatalytic activity of CPs.

18. Alonso Vante N, Schubert B, Tributsch H: **Transition metal cluster materials for multi-electron transfer**. *Mater Chem Phys* 1989, **22**:281–307, https://doi.org/10.1016/0254-0584(89)90002-3.

19. Strachan J, Masters AF, Maschmeyer T: **Chevrel Phase nanoparticles as electrocatalysts for hydrogen evolution**. *ACS Appl Nano Mater* 2021, **4**:2030–2036, https://doi.org/10.1021/acsanm.0c03355.

20. * Schubert B, Tributsch H: **Single-metal catalytic centers for hydrogen evolution**. *J Electrochem Soc* 1993, **140**:98–103, https://doi.org/10.1149/1.2056117.
The study identified that HER in CPs is dominated by a single metal catalytic center. The evaluation of different CP compositions for HER is one of the first examples of structure function studies in CPs.

21. Naik KM, Sampath S: **Cubic Mo6S8-efficient electrocatalyst towards hydrogen evolution over wide pH range**. *Electrochim Acta* 2017, **252**:408–415, https://doi.org/10.1016/j.electacta.2017.09.015.

22. ** Ortiz-Rodríguez JC, Singstock NR, Perryman JT, Hyler FP, Sarah J, Holder AM, Musgrave B, Velázquez JM: **Stabilizing hydrogen adsorption through theory-guided chalcogen substitution in Chevrel-phase Mo6X8 (X = S , Se , Te) electrocatalysts**. *ACS Appl Mater Interfaces* 2020, **12**:35995–36003, https://doi.org/10.1021/acsami.0c07207.
The study evaluated the changes in HER activity in CPs as a function of chalcogen. It is the first study that combines experiment and theory to provide a complete understanding of the changes in H adsorption in CP chalcogenides.

23. Elgendy A, Papaderakis AA, Byrne C, Sun Z, Lauritsen Jv, Higgins EPC, Ejigu A, Cernik R, Walton AS, Lewis DJ, Dryfe RAW: **Nanoscale Chevrel-phase Mo6S8 prepared by a molecular precursor approach for highly efficient electrocatalysis of the hydrogen evolution reaction in acidic media**. *ACS Appl Energy Mater* 2021, https://doi.org/10.1021/acsaem.1c02646.

24. Ojha K, Banerjee S, Sharma M, Dagar P: **Synthesis of Chevrel phase (Cu61.8Mo6S8) in composite with molybdenum carbide for hydrogen evolution reactions**. *Bull Mater Sci* 2018, **41**:1–7, https://doi.org/10.1007/s12034-018-1633-z.

25. Jiang J, Gao M, Sheng W, Yan Y: **Hollow Chevrel-phase NiMo3S4 for hydrogen evolution in alkaline electrolytes**. *Angew Chem* 2016, **128**:15466–15471, https://doi.org/10.1002/ange.201607651.

26. Zhang Q, Guo L, Hao Z: **Computational investigation of M1/W6S8 (M = Fe, Ru, and Os) single-atom catalysts for CO2 hydrogenation**. *Catal Surv Asia* 2018, **22**:195–207, https://doi.org/10.1007/s10563-018-9252-7.

27. Zhang Q, Guo L, Hao Z: **Exploration of high-performance W6S8-supported single-atom Rh1 catalysts for reverse water–gas shift reaction and methanol formation via DFT computational study**. *Polyhedron* 2018, **146**:108–120, https://doi.org/10.1016/j.poly.2018.01.025.

28. Zheng X, Guo L, Li W, Cao Z, Liu N, Zhang Q, Xing M, Shi Y, Guo J: **Insight into the mechanism of reverse water-gas shift reaction and ethanol formation catalyzed by Mo6S8-TM clusters**. *Mol Catal* 2017, **439**:155–162, https://doi.org/10.1016/j.mcat.2017.06.030.

29. ** Liu C, Liu P: **Mechanistic study of methanol synthesis from CO2 and H2 on a modified model Mo6S8 cluster**. *ACS Catal* 2015, **5**:1004–1012, https://doi.org/10.1021/cs501354b.
The authors evaluated CO_2 reduction to methanol on a variety of metal intercalated CPs. An extensive discussion of ligand and ensemble effect in these materials is provided.

30. ** Perryman JT, Ortiz-Rodríguez JC, Jude JW, Hyler FP, Davis RC, Mehta A, Kulkarni AR, Patridge CJ, Velázquez JM: **Metal-promoted Mo6S8 clusters: a platform for probing ensemble effects on the electrochemical conversion of CO2 and CO to methanol**. *Mater Horiz* 2020, **7**:193–202, https://doi.org/10.1039/c9mh00745h.
The authors evaluated Mo_6S_8 and MMo_6S_8 (M = Cr, Cu, Ni) as electrocatalyst for CO_2RR. This is the first experimental validation of computational work that predicted that CPs could reduce CO_2 to methanol.

31. ** Liu P, Choi Y, Yang Y, White MG: **Methanol synthesis from H2 and CO2 on a Mo 6S8 cluster: a density functional study**. *J Phys Chem A* 2010, **114**:3888–3895, https://doi.org/10.1021/jp906780a.
This study provides the first computational prediction regarding the ability of Mo_6S_8 to reduce CO_2 to methanol. Rate limiting steps and favorable active sites are identified.

32. Cao Z, Guo L, Liu N, Zheng X, Li W, Shi Y, Guo J, Xi Y: **Theoretical study on the reaction mechanism of reverse water-gas shift reaction using a Rh-Mo6S8 cluster**. *RSC Adv* 2016, **6**:108270–108279, https://doi.org/10.1039/c6ra23855f.

33. ** Lu K, Xia F, Li B, Liu Y, Abdul Razak IB, Gao S, Kaelin J, Brown DE, Cheng Y: **Synergistic multisites Fe2Mo6S8 electrocatalysts for ambient nitrogen conversion to ammonia**. *ACS Nano* 2021, **15**:16887–16895, https://doi.org/10.1021/acsnano.1c07771.
This is the first work to evaluate Mo_6S_8 and $M_2Mo_6S_8$ (M = Cu, Mn, Fe) as electrocatalyst for NRR. $Fe_2Mo_6S_8$ shows significant NH_3 conversion, which is hypothesized to be due the improved ensemble effect of Fe compared to the other CPs studied.

34. Pérez-Ramírez J, López N: **Strategies to break linear scaling relationships**. *Nat Catal* 2019, **2**:971–976, https://doi.org/10.1038/s41929-019-0376-6.

35. He J, Johnson NJJ, Huang A, Berlinguette CP: **Electrocatalytic alloys for CO2 reduction**. *ChemSusChem* 2018, **11**:48–57, https://doi.org/10.1002/cssc.201701825.

36. Lee CW, Yang KD, Nam DH, Jang JH, Cho NH, Im SW, Nam KT: **Defining a materials database for the design of copper binary alloy catalysts for electrochemical CO2 conversion**. *Adv Mater* 2018, **30**:1704717, https://doi.org/10.1002/adma.201704717.

37. Hill CM, Mendoza-Cortes JL, Velazquez JM, Whittaker-Brooks L: **Multi-dimensional designer catalysts for negativeemissions science (NES): bridging the gap between synthesis, simulations, and analysis**. *iScience* 2020, **23**:101152, https://doi.org/10.1016/j.isci.

38. Nørskov JK, Abild-Pedersen F, Studt F, Bligaard T: **Density functional theory in surface chemistry and catalysis**. *Proc Natl Acad Sci Unit States Am* 2011, **108**:937–943, https://doi.org/10.1073/pnas.1006652108.

39. Hammer B, Norskov JBK: **Electronic factors determining the reactivity of metal surfaces**. *Surf Sci* 1995, **343**:211–220.

40. Hammer B, Nørskov JK: **Theoretical surface science and catalysis-calculations and concepts**. *Adv Catal* 2000, **45**: 71–129, https://doi.org/10.1016/0039-6028(96)80007-0.

41. Lee YL, Kleis J, Rossmeisl J, Yang SH, Morgan D: **Prediction of solid oxide fuel cell cathode activity with first-principles descriptors**. *Energy Environ Sci* 2011, **4**:3966–3970, https://doi.org/10.1039/c1ee02032c.

42. Hong WT, Stoerzinger KA, Lee YL, Giordano L, Grimaud A, Johnson AM, Hwang J, Crumlin EJ, Yang W, Shao-Horn Y: **Charge-transfer-energy-dependent oxygen evolution reaction mechanisms for perovskite oxides**. *Energy Environ Sci* 2017, **10**:2190–2200, https://doi.org/10.1039/c7ee02052j.

43. ** Zhao ZJ, Liu S, Zha S, Cheng D, Studt F, Henkelman G, Gong J: **Theory-guided design of catalytic materials using scaling relationships and reactivity descriptors**. *Nat Rev Mater* 2019, **4**:792–804, https://doi.org/10.1038/s41578-019-0152-x.
The review describes the influence of reactivity descriptors in the progress of improved catalyst materials. An overview of the established reactivity descriptors is given along future directions to increase catalyst performance.

44. Jaegermann W, Pettenkofer C, Alonso Vante N, Schwarzlose Th, Tributsch H: **Chevrel phase type compounds: electronic, chemical and structural factors in oxygen reduction electrocatalysis**. *Ber Bunsenges Phys Chem* 1990, **94**:513–520, https://doi.org/10.1002/bbpc.19900940416.

45. Alonso Vante N: **Chevrel phases and chalcogenides**. In *Handbook of fuel cells : fundamentals, technology, and applications*. John Wiley & Sons; 2003:534–543.

46. Zhang L, Zhang J, Wilkinson DP, Wang H: **Progress in preparation of non-noble electrocatalysts for PEM fuel cell reactions**. *J Power Sources* 2006, **156**:171–182, https://doi.org/10.1016/j.jpowsour.2005.05.069.

47. Lee JW, Popov BN: **Ruthenium-based electrocatalysts for oxygen reduction reaction-a review**. *J Solid State Electrochem* 2007, **11**:1355–1364, https://doi.org/10.1007/s10008-007-0307-3.

48. Mora-Hernández J, Luo Y, Alonso Vante N, Mora-Hernández JM: **What can we learn in electrocatalysis, from nanoparticulated precious and/or non-precious catalytic centers interacting with their support?** *Catalysts* 2016, **6**:1–55, https://doi.org/10.3390/catal6090145ï.

49. Strachan J, Masters AF, Maschmeyer T: **The catalytic nature of Chevrel phases (MxMo6S8) in review**. *Mater Res Bull* 2021, **139**:111286, https://doi.org/10.1016/j.materresbull.2021.111286.

50. Li F, Han GF, Noh HJ, Jeon JP, Ahmad I, Chen S, Yang C, Bu Y, Fu Z, Lu Y, Baek JB: **Balancing hydrogen adsorption/desorption by orbital modulation for efficient hydrogen evolution catalysis**. *Nat Commun* 2019, **10**:4060, https://doi.org/10.1038/s41467-019-12012-z.

51. Wang J, Liu J, Zhang B, Ji X, Xu K, Chen C, Miao L, Jiang J: **The mechanism of hydrogen adsorption on transition metal dichalcogenides as hydrogen evolution reaction catalyst**. *Phys Chem Chem Phys* 2017, **19**:10125–10132, https://doi.org/10.1039/c7cp00636e.

52. Zheng X, Guo S, Guo L: **Ethanol synthesis catalyzed by single Ni atom supported on Mo6S8 support**. *Appl Catal Gen* 2018, **553**:52–64, https://doi.org/10.1016/j.apcata.2018.01.010.

53. Hughbanks Timothy, Hoffmann Roald: **Molybdenum chalcogenides: clusters, chains, and extended solids. The approach to bonding in three dimensions**. *J Am Chem Soc* 1983, **105**: 1150–1162, https://doi.org/10.1021/ja00343a014.

54. Andersen OK, Klose W, Nohl H: **Electronic structure of Chevrel-phase high-critical-field superconductors**. *Phys Rev B* 1978, **17**:1209–1237, https://doi.org/10.1103/PhysRevB.17.1209.

55. **Fischer: Chevrel phases: superconducting and normal state properties**. *Appl Phys Res* 1978, **16**:1–28, https://doi.org/10.1007/BF00931416.

56. Bullett DW: **Relation between electronic structure and Tc in binary and ternary molybdenum chalcogenides**. *Phys Rev Lett* 1977, **39**:664–666, https://doi.org/10.1103/PhysRevLett.39.664.

57. Yvon K, Paoli A: **Charge transfer and valence electron concentration in Chevrel phases**. *Solid State Commun* 1977, **24**: 41–45, https://doi.org/10.1016/0038-1098(77)90561-0.

58. Mccallum RW, Pobell F, Shelton RN: **125 Te Mossbauer effect in Chevrel phase compounds Mo6(Se1-x Tex)8**. *Phys Lett* 1982, **89**:316–318.

59. Berry FJ, Gibbs C: **Bonding in Mo4.5Ru1.5Te8, Ni0.85Mo6Te8, Chevrel phase, and related compounds**. *J Solid State Chem* 1994, **109**:22–29, https://doi.org/10.1016/0375-9601(82)90866-0.

60. Sergent M, Fischer Q, Decroux M, Perrin C, Chevrel R: **Stabilization of Mo6S8 by halogens; New superconducting compounds: Mo6SaBr2, Mo6S6I2**. *J Solid State Chem* 1977, **22**: 87–92, https://doi.org/10.1016/0022-4596(77)90192-X.

61. Hamard C, Auffret V, Pena O, le Floch M, Nowak B, Wojakowski A: **Chevrel-phase solid solution Mo6Se8-xTex. Study of its superconducting, magnetic and NMR properties**. *Phys B* 1999, **291**: 339–349, https://doi.org/10.1016/S0921-4526(99)02286-3.

62. Wang J, Li X, Wei B, Sun R, Yu W, Hoh HY, Xu H, Li J, Ge X, Chen Z, Su C, Wang Z: **Activating basal planes of NiPS3 for hydrogen evolution by nonmetal heteroatom doping**. *Adv Funct Mater* 2020, **30**:1908708, https://doi.org/10.1002/adfm.201908708.

63. Zhang B, Fu X, Song L, Wu X: **Computational screening toward hydrogen evolution reaction by the introduction of point defects at the edges of group IVA monochalcogenides: a first-principles study**. *J Phys Chem Lett* 2020, **11**:7664–7671, https://doi.org/10.1021/acs.jpclett.0c02047.

64. Wang Y, Wang D, Gao J, Hao X, Li Z, Zhou J, Gao F: **Optimized electronic structure and p-band centre control engineering to enhance surface absorption and inherent conductivity for accelerated hydrogen evolution over a wide pH range**. *Phys Chem Chem Phys* 2020, **22**:14537–14543, https://doi.org/10.1039/d0cp02131h.

65. Yang T, Xie H, Ma N, Liu E, Shi C, He C, Zhao N: **Unraveling the mechanism of hydrogen evolution reaction on cobalt compound electrocatalysts**. *Appl Surf Sci* 2021, **550**:1–9, https://doi.org/10.1016/j.apsusc.2021.149355.

66. Perryman JT, Hyler FP, Ortiz-Rodríguez JC, Mehta A, Kulkarni AR, Velázquez JM: **X-ray absorption spectroscopy study of the electronic structure and local coordination of 1st row transition metal-promoted Chevrel-phase sulfides**. *J Coord Chem* 2019, **72**:1322–1335, https://doi.org/10.1080/00958972.2019.1613532.

67. Wan LF, Wright J, Perdue BR, Fister TT, Kim S, Apblett CA, Prendergast D: **Revealing electronic structure changes in Chevrel phase cathodes upon Mg insertion using X-ray absorption spectroscopy**. *Phys Chem Chem Phys* 2016, **18**: 17326–17329, https://doi.org/10.1039/c6cp02412b.

68. Thole F, Wan LF, Prendergast D: **Re-examining the Chevrel phase Mo6S8 cathode for Mg intercalation from an electronic structure perspective**. *R Soc Chem* 2015, **19**:22548–22551, https://doi.org/10.1039/x0xx00000x.

69. Berry FJ, Gibbs CD, Greaves C: **Structural properties of the molybdenum-ruthenium telluride of composition**. *J Solid State Chem* 1991, **92**:148–153, https://doi.org/10.1016/0022-4596(91)90251-C.

70. Chevrel R, Gougeon P, Potel M, Sergent M: **Ternary molybdenum chalcogenides: a route to new extended clusters**. *J Solid State Chem* 1985, **57**:25–33, https://doi.org/10.1016/S0022-4596(85)80057-8.

71. Jaegermann W, Tributsch H: **Interfacial properties of semiconducting transition metal chalcogenides**. *Prog Surf Sci* 1988, **29**:1–167, https://doi.org/10.1016/0079-6816(88)90015-9.

72. Guo L, Han Y, Guo S: **Synthesis gas conversion over Cu and Ca modified model Mo6S8 catalysts: a systematic theoretical investigation**. *Int J Hydrogen Energy* 2020, **45**:12798–12814, https://doi.org/10.1016/j.ijhydene.2020.02.224.

73. Singstock NR, Ortiz-Rodríguez JC, Perryman JT, Sutton C, Velázquez JM, Musgrave CB: **Machine learning guided synthesis of multinary Chevrel phase chalcogenides**. *J Am Chem Soc* 2021, **143**:9113–9122, https://doi.org/10.1021/jacs.1c02971.

74. Lilova K, Perryman JT, Singstock NR, Abramchuk M, Subramani T, Lam A, Yoo R, Ortiz-Rodríguez JC, Musgrave CB, Navrotsky A, Velázquez JM: **A synergistic approach to unraveling the thermodynamic stability of binary and ternary Chevrel phase sulfides**. *Chem Mater* 2020, **32**:7044–7051, https://doi.org/10.1021/acs.chemmater.0c02648.

75. Mançour-Billah A, Chevrel R: **The transition element sulfoselenide Chevrel phases: a new way to stabilize the Mo6(S,Se)8 framework**. *J Alloys Compd* 2004, **383**:49–56, https://doi.org/10.1016/j.jallcom.2004.04.007.

76. Belin S, Chevrel R, Sergent M: **Single crystal structural investigations on Ni(y)Mo6Se(8-x)S(x) solid solution: a new location of nickel counterions**. *J Solid State Chem* 2000, **155**: 250–258, https://doi.org/10.1006/jssc.2000.8961.

77. Mancour-Billah A, Gougeon P, Pivan JY, Sergent M, Chevrel R: **New type-structure of Chevrel phase: unusual location of the 3d chromium ions in the Mo6S8 host lattice**. *Croat Chem Acta* 1995, **68**:891–899.

78. Levi E, Gershinsky G, Aurbach D, Isnard O, Ceder G: **New insight on the unusually high ionic mobility in Chevrel phases**. *Chem Mater* 2009, **21**:1390–1399, https://doi.org/10.1021/cm900033v.

79. Yvon K: **On the lattice instabilities in Chevrel phases**. *Solid State Commun* 1978, **25**:327–331, https://doi.org/10.1016/0038-1098(78)90969-9.

80. Levi E, Gershinsky G, Aurbach D, Isnarcr O: **Crystallography of Chevrel phases, MMo6T8 (M = Cd, Na, Mn, and Zn, T = S, Se) and their cation mobility**. *Inorg Chem* 2009, **48**:8751–8758, https://doi.org/10.1021/ic900805g.

81. Arán-Ais RM, Rizo R, Grosse P, Algara-Siller G, Dembélé K, Plodinec M, Lunkenbein T, Chee SW, Roldan Cuenya B: **Imaging electrochemically synthesized Cu2O cubes and their morphological evolution under conditions relevant to CO2 electroreduction**. *Nat Commun* 2020, **11**:3489, https://doi.org/10.1038/s41467-020-17220-6.

82. Li Y, Kim D, Louisia S, Xie C, Kong Q, Yu S, Lin T, Aloni S, Fakra SC, Yang P: **Electrochemically scrambled nanocrystals are catalytically active for CO 2-to-multicarbons**. *Proc Natl Acad Sci Unit States Am* 2020, **117**:9194–9201, https://doi.org/10.1073/pnas.1918602117/-/DCSupplemental.

83. Kim YG, Baricuatro JH, Soriaga MP: **Surface reconstruction of polycrystalline Cu electrodes in aqueous KHCO3 electrolyte at potentials in the early stages of CO2 reduction**. *Electrocatalysis* 2018, **9**:526–530, https://doi.org/10.1007/s12678-018-0469-z.

84. Hahn C, Hatsukade T, Kim YG, Vailionis A, Baricuatro JH, Higgins DC, Nitopi SA, Soriaga MP, Jaramillo TF: **Engineering Cu surfaces for the electrocatalytic conversion of CO2: controlling selectivity toward oxygenates and hydrocarbons**. *Proc Natl Acad Sci Unit States Am* 2017, **114**:5918–5923, https://doi.org/10.1073/pnas.1618935114.

85. Yang Y, Xiong Y, Zeng R, Lu X, Krumov M, Huang X, Xu W, Wang H, Disalvo FJ, Brock JD, Muller DA, Abrunã HD: **Operando methods in electrocatalysis**. *ACS Catal* 2021, **11**:1136–1178, https://doi.org/10.1021/acscatal.0c04789.

86. Timoshenko J, Roldan Cuenya B: **In Situ/operando electrocatalyst characterization by x-ray absorption spectroscopy**. *Chem Rev* 2021, **121**:882–961, https://doi.org/10.1021/acs.chemrev.0c00396.

87. Monteiro MCO, Mirabal A, Jacobse L, Doblhoff-Dier K, Barton SC, Koper MTM: **Time-resolved local pH measurements during CO2 reduction using scanning electrochemical microscopy: buffering and tip effects**. *J Am Chem Soc Au* 2021, **1**:1915–1924, https://doi.org/10.1021/jacsau.1c00289.

88. Mayer FD, Hosseini-Benhangi P, Sánchez-Sánchez CM, Asselin E, Gyenge EL: **Scanning electrochemical microscopy screening of CO2 electroreduction activities and product selectivities of catalyst arrays**. *Comm Chem* 2020, **3**:155, https://doi.org/10.1038/s42004-020-00399-6.

89. Clark EL, Singh MR, Kwon Y, Bell AT: **Differential electrochemical mass spectrometer cell design for online quantification of products produced during electrochemical reduction of CO2**. *Anal Chem* 2015, **87**:8013–8020, https://doi.org/10.1021/acs.analchem.5b02080.

90. Bondue CJ, Koper MTM: **A DEMS approach for the direct detection of CO formed during electrochemical CO2 reduction**. *J Electroanal Chem* 2020, **875**:113842, https://doi.org/10.1016/j.jelechem.2020.113842.

91. Yao Y, Zhu S, Wang H, Li H, Shao M: **A spectroscopic study of electrochemical nitrogen and nitrate reduction on rhodium surfaces**. *Angew Chem Int Ed* 2020, **59**:10479–10483, https://doi.org/10.1002/anie.202003071.

92. Zeng L, Li X, Chen S, Wen J, Huang W, Chen A: **Unique hollow Ni-Fe@MoS2 nanocubes with boosted electrocatalytic activity for N2 reduction to NH3**. *J Mater Chem A* 2020, **8**: 7339–7349, https://doi.org/10.1039/c9ta13336d.

93. Firet NJ, Smith WA: **Probing the reaction mechanism of CO2 electroreduction over Ag films via operando infrared spectroscopy**. *ACS Catal* 2017, **7**:606–612, https://doi.org/10.1021/acscatal.6b02382.

94. Zhu S, Li T, Cai W bin, Shao M: **CO2 electrochemical reduction as probed through infrared spectroscopy**. *ACS Energy Lett* 2019, **4**:682–689, https://doi.org/10.1021/acsenergylett.8b02525.

95. Kalz KF, Kraehnert R, Dvoyashkin M, Dittmeyer R, Gläser R, Krewer U, Reuter K, Grunwaldt JD: **Future challenges in heterogeneous catalysis: understanding catalysts under dynamic reaction conditions**. *ChemCatChem* 2017, **9**:17–29, https://doi.org/10.1002/cctc.201600996.

96. Frenkel AI, Rodriguez JA, Chen JG: **Synchrotron techniques for in situ catalytic studies: capabilities, challenges, and opportunities**. *ACS Catal* 2012, **2**:2269–2280, https://doi.org/10.1021/cs3004006.

97. Weckhuysen BM: **Determining the active site in a catalytic process: operando spectroscopy is more than a buzzword**. *Phys Chem Chem Phys* 2003:4351–4360, https://doi.org/10.1039/b309650p.

98. Portela R, Perez-Ferreras S, Serrano-Lotina A, Bañares MA: **Engineering operando methodology: understanding catalysis in time and space**. *Front Chem Sci Eng* 2018, **12**:509–536, https://doi.org/10.1007/s11705-018-1740-9.

99. Negahdar L, Parlett CMA, Isaacs MA, Beale AM, Wilson K, Lee AF: **Shining light on the solid-liquid interface: in situ/operando monitoring of surface catalysis**. *Catal Sci Technol* 2020, **10**:5362–5385, https://doi.org/10.1039/d0cy00555j.